A 3D reconstruction-based method using unmanned aerial vehicles for the representation and analysis of road sections

Brahim Benmhahe, Jihane Alami Chentoufi, Mohamed Amine Basmassi
Laboratory of Computer Science Research, Faculty of Sciences, Ibn Tofail University, Kenitra, Morocco

Article Info

ABSTRACT

Due to the fast growth of cities worldwide, roads are increasing daily, and pavement maintenance has become very heavy and costly. Despite all efforts made under the pavement management system to keep the road surface in good shape, several road sections need to be in better condition, which presents a danger for drivers and pedestrians. This paper proposes a novel pavement 3D reconstruction and segmentation approach using the structure from motion technique, unmanned aerial vehicle, and digital camera. The method consists of the 3D modeling of the road by using images taken from different perspectives and the structure from motion technique. In this method, points cloud is sampled and cleaned using statistical outlier removal and noise filters. After that, duplicated and isolated points are eliminated to retain only significant data. The normal road plane is estimated using the principal component analysis technique and the remaining points. This plan presents a root mean square less than 0.85 cm. Finally, distances from those points to the normal plane are calculated and clustered to segment the road into distressed and non-distressed areas. The proposed approach presents a similarity rate to the survey measurement passed 95%. It has demonstrated promising results and has the potential for further improvement by optimizing various steps.

Corresponding Author:

Brahim Benmhahe
Laboratory of Computer Science Research, Faculty of Sciences, Ibn Tofail University
Kenitra, Morocco
Email: Brahim.benmhahe@uit.ac.ma

1. INTRODUCTION

There is no doubt that pavement damage is a critical situation that cannot be avoided either in a road city or at the runway airport. This fact is due to factors such as environmental parameter changes (temperature and pressure), aging, vehicle overloads, initial poor construction, and the absence or the existence of low maintenance quality. Pavement maintenance must be done in a timely and specific manner to ensure safety, avoid accidents, permit minimum comfort for road users, save vehicles from deterioration, and prevent pavement maintenance from becoming heavy and costly.

In this regard, the pavement management system (PMS) concept was introduced in 1970 to monitor the pavement's health and define when and how to maintain it, considering resource optimization and keeping the pavement surface in good shape for as long as possible. Initially, PMS was based on handbooks, classical measurement tools, and human observation, which is considered time-consuming, subject to observer bias and tool limitation, and presenting multiple dangers for observers, pedestrians, and drivers during data acquisition. To overcome such limitations, various approaches have been adopted and developed over time, as evidenced by numerous research studies and publications in this field [1]–[3]. With the advent of smart city technology, PMS has been enhanced to include the latest advanced material and tools such as

cameras, laser scanners, and other sensors such as accelerometers, vibration, and acoustic to monitor in real-time the pavement surface [4]–[6]. After data acquisition, several artificial intelligence and machine learning algorithms [7]–[12] were adapted and enhanced to analyze data gathered and extract meaningful information to detect, measure, and classify pavement distress.

Regarding the nature of data acquired, the research could be classified into three categories: vibration-based, vision-based, and 3D scanning-based. Vibration-based consists of using accelerometers, vibration, and acoustic sensors for data acquisition [13]. Thus, damages on pavement cause a non-desired vertical and horizontal movement of the tire, which could be captured by installing such sensors on a vehicle. Some solutions were proposed to measure acceleration data by installing smartphone accelerometers on cars [14]–[16]. However, these solutions present limitations regarding the absence of significant data and the difficulties of gathering data in traffic congestion. Also, vibration data are received mainly via tire behavior, and damages not traversed by the tire could not be captured. Vibration-based methods have been disregarded for those reasons and others [12]. The second concept is the vision-based method of capturing images or videos with a camera, smartphone, or unmanned aerial vehicle (UAV). Several researchers intensely studied this method by adapting and enhancing multiple artificial intelligence and machine learning algorithms to extract pavement damage from images [17]–[23]. However, images present just two dimensions of information, and the third dimension (depth) cannot be extracted. The vision-based method is practical for detecting and measuring damage, characterized by two significant dimensions (cracks) and identifying and localizing other damages, such as potholes and rutting. Despite the high accuracy achieved by the vision-based method for crack detection and measurement (around 95%) [24], the importance of the depth information for other types of damage is the main reason that drives researchers to look for other methods. The third and last concept consists of the 3D scanning of the road using laser scanners, light detection sensors, or other methods that offer high accuracy and present more significant data. 3D scanning helps to accurately measure all pavement damages, such as cracks, ruts, potholes, and wash-boarding [25]–[27]. However, the 3D scanning of the pavement is very costly, time-consuming, and stops traffic during the scan.

Road 3D modeling is the more adapted solution that will permit extracting all necessary data with the minimum precision to overcome the abovementioned limitations. However, it should be less costly, more flexible, and ensure safety for all involved parties. Bruno *et al.* [28] proposed a low-cost pothole monitoring system based on a camera and global positioning system (GPS) modules managed by a mini-computer Raspberry Pi 4B. Collected images were processed through photogrammetric techniques to create the pothole 3D model and calculate the volume of asphalt to fill. In this regard, the present paper proposes a novel approach based on the structure from motion (SFM) technique, a low-cost UAV, and a commercial digital camera for road 3D modeling and segmentation. 3D points are extracted and processed to remove almost unnecessary data, including noise. The normal plan, which represents the road surface plan before damages, is estimated based on the remaining points and the principal component analysis (PCA) technique. After that, damaged areas are defined based on distances between 3D points and the normal plane. A case study with a complicated, damaged pavement will be used to evaluate the proposed approach.

The remaining sections are organized as follows: section 2 describes the state-of-the-art research studies in pavement 3D reconstruction and distress detection using the SFM technique and UAVs. The flowchart of the study outlining the various steps involved in implementing the proposed method will be described in section 3. Then, section 4 will present the material used with the experimental results and discussion. The paper will be concluded in section 5, and a summary of the key findings will be presented.

2. BACKGROUND

During the literature review, it was observed that using UAVs to asses pavement health is a prevalent technique [29], which presents more flexibility and guarantees safety for observers, pedestrians, and drivers. Among UAVs, the Da Jiang Innovation (DJI) family was the most efficient due to their superior navigation and optical systems, including high-quality cameras, as illustrated in Table 1. Also, it can be considered a low-cost solution compared to the vehicle used for road scanning. Furthermore, the SFM was identified as the commonly used technique for pavement 3D modeling, which is very robust and accurate. Then, multiple software and algorithms (singular value decomposition, canny edge, Hough circle transform, and Gabor filtering) are applied to the 3D model to isolate the road from other objects, detect damaged areas, and perform measurement and classification. However, existing methods still present some limitations regarding the low quality of data gathered, no detection and localization of damages, no identification of the type of distress (pothole, rut, and wash-boarding), no measurement of the distress or the measurement done manually, and no classification of the severity of damages [30]–[38]. To our knowledge, research is still being concluded on automatically detecting, measuring, and classifying damages in road networks. Table 1 illustrates recent research studies that used UAVs and SFM techniques to evaluate

pavement health, providing a comprehensive overview of the current state-of-the-art in this field and presenting the limitations of each method.

Table 1. Recent research based on UAVs and SFM to evaluate pavement health

Reference	Material	Software and Algorithms	Limitations
[29]	DJI P4RTK	*SFM *Bundle adjustment *Pix4DMapper *Convex hull *Density based spatial clustering of applications with noise (DBSCAN)	*No identification *No classification
[30]	Helicopter drone with Canon EOS Rebel XT camera	*SFM	*Low-quality data *No detection *No identification *No measurement *No classification
[31]	TAZER 800 HELICOPTER with Nikon D800 Camera	*SFM *Patch-based multi-view stereo *Windowed entropy filter *Singular value decomposition *Canny edge detection *Hough circle transform *Gabor filtering	*Detection and identification of only potholes and wash-boarding *No measurement *No classification
[32]	DJI Mavric Pro 2	*SFM *MetaShape *CloudCompare *Random sample consensus (RANSAC) *2.5D Quadric Fit	*No detection *No identification
[33]	DJI P4RTK	*SFM *Pix4DMapper *GlobalMapper *Scale invariant feature transform (SIFT) *Multi view stereo (MVS)	*Detection and identification of only ruts and potholes *Manual measurement *No classification
[34]	Phantom 4 Pro	*Pix4Dmapper *Region growing *Statistical outlier removal (SOR) *Graham Scan	*No identification *No classification
[35]	DJI Mavic Pro	*SFM *Pix4Dmapper *PhotoScan *SIFT	*Detection and identification of only potholes *No classification
[36]	DJI Phantom 3 Quadcopter	*PhotoScan. *GlobalMapper.	*Detection and identification of only potholes and ruts *Manual measurement *No classification
[37]	UAV equipped with GoPro Hero3	*SFM *PhotoScan *MeshLab *Rhinoceros CAD	*No identification *No measurement *No classification

3. METHOD

In this section, the flow chart of the study will be presented, and each step of the method will be described after explaining the software and algorithms used. This study aims to utilize a cutting-edge approach for road 3D reconstruction and segmentation using a UAV and a digital camera to take images of the road. Those images will then be processed and transformed into 3D models using the SFM technique. Furthermore, a developed algorithm will isolate the road from other objects in the scene and accurately make a 3D representation of the inspected road segment. This algorithm can handle damages such as potholes, ruts, and wash-boarding. Figure 1 provides a clear and concise flow chart of the study outlining the main steps involved in the proposed method, from data acquisition to final analysis and road segmentation to distressed and non-distressed areas.
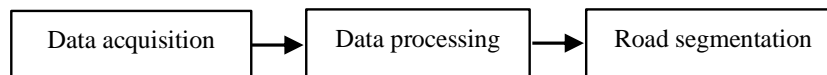
Data acquisition → Data processing → Road segmentation

Figure 1. Flow chart of the study

3.1. Software and algorithms

3.1.1. Structure from motion

Photogrammetry is a science that aims to extract information and measurements from photographs through processes and patterns. It is a well-established technique used in various fields such as surveying, cartography, and remote sensing [39], [40]. Structure from Motion is one of the most recent and widely used photogrammetry techniques [41]. SFM enables the creation of 3D models using overlapping images acquired from different perspectives with standard cameras, including Smartphone cameras. It is based on recovering the 3D structure of a stationary scene by collecting 2D images and estimating the cameras' motion corresponding to these images. SFM employs various algorithms and techniques, such as scale invariant feature transform (SIFT), random sample consensus (RANSAC), and bundle adjustment.

SFM process involves four main steps: i) features extraction from images: points of interest, edges, and corners, ii) features matching between images, iii) camera pose estimation based on the extracted features, and iv) 3D model reconstruction using the estimated poses and features. These steps enable SFM to generate accurate and more detailed 3D models of the scene, allowing for precise measurement and analysis of the captured images. SFM has been approved as an appropriate technique for pavement 3D modeling. Several algorithms and software are built based on the SFM (VisualSFM [42], Bundler [43], Pix4D [44], RealityCapture [45], and Agisoft [46]). However, it could be enhanced by introducing other techniques, especially feature extraction, feature matching, and image matching steps. Meshroom is considered one of the most powerful algorithms based on the SFM technique.

3.1.2. Meshroom

Meshroom [47] is powerful 3D reconstruction software based on the AliceVision framework. The software is available in two versions: application with graphical user interface (GUI) and open-source algorithm, which can be modified and adapted to meet user requirements. It is open-source for the three major operating systems: Windows, Linux, and macOS. Meshroom is based on the SFM technique and employs other algorithms and techniques such as SIFT, RANSAC, and Accelerated KAZE (AKAZE). GUI application requires a computer with an Nvidia graphics processing unit (GPU), with a compute capability of at least 2.0, for the dense, high-quality mesh generation and 32GB of random-access memory (RAM) for the meshing. However, adjusting parameters and bypassing all nodes that require those characteristics is possible. In order to avoid any computer limitations, the last stable software (version 2021.1.0 Linux) was personalized and run via the virtual platform Google Colab [48].

3.1.3. CloudCompare

CloudCompare [49] is a multipurpose 3D points cloud, meshes editing and processing software widely used in various fields such as geology, archaeology, architecture, and engineering. It can compare points cloud with Mesh data and provide good analysis. This software provides multiple processing algorithms, including SOR, noise filters, resampling, color/normal and vectors/scalar management, statistical computation, and sensor management. The software presents an intuitive GUI and is plugged into algorithms such as Hough normal, RANSAC shape detection, multiscale model-to-model cloud comparison (M3C2), and others. This plug-in can perform tasks such as normal estimation, shape detection, points cloud cleaning,

plane fitting, and surface reconstruction. Additionally, it is possible to plug in other algorithms when necessary for specific tests or applications.

3.2. Data acquisition

This step starts with defining the limitation geographic of the road area to be inspected. After that, data acquisition is made by a commercial camera or a low-cost UAV. This step is the most critical and challenging part of the process. It significantly impacts the precision and accuracy of road 3D modeling and segmentation. For this reason, images should be taken from different angles with an overlap of 70% to cover the whole section and meet the 3D modeling redundancy requirements. Devices should be configured, considering environmental parameters (temperature and lighting) and distance to the pavement, guaranteeing clear and not blurred images.

3.3. Data processing

This step takes raw pavement images as input and produces a clean 3D points cloud, representing the pavement section concerned by the inspection. Data processing is critical because it corrects errors during data collection, and the accuracy of its output directly impacts the accuracy of the road segmentation step. Data processing consists of six sub-steps, as illustrated in Figure 2: 3D modeling, points cloud extraction, road extraction, outliers' removal, noise removal, and duplicated points removal.

Road 3D modeling is created using Meshroom. Points cloud extraction is done on CloudCompare to remove meshes from the 3D model and keep only 3D points; the total number of existing points was sampled to keep all data at this level. Road extraction consists of eliminating all objects and keeping only the section of the road to be inspected; the criteria used to eliminate non-road objects is the z coordinate; all points with a *z* value greater than 0.5 m were considered a non-road object and eliminated.

Outlier removal: the statistical outlier removal filter was applied to points, representing the road, to remove outliers. SOR first calculates each point's average distance to its nearest neighbors. Then, it eliminates the points farther than a certain number of standard deviations from the average distances, as defined by (1).

$$Max\ d = Avg\ d\ + (N.Std\ Dv) \tag{1}$$

$Max\ d$ is the maximum distance allowed from a given point, $Avg\ d$ is the average distance between the given point and its K nearest neighbors, $Std\ Dv$ is the standard deviation of the average distances, and N is the number of times of standard deviations.

Noise removal: existing noises make false 3D modeling and reduce the accuracy of road segmentation. This sub-step eliminates unnecessary data to keep the minimum required and the more confident points. This algorithm locally fits a sphere plane with a radius of 0.9 cm around each point and removes all points far away from the fitted plane. Isolated points are also removed at this stage. A point is considered isolated when less than three neighbors exist on the fitted sphere. Duplicated points removal consists of eliminating 3D points based on a minimum distance criterion. If the distance between two points is less than 0.005 cm, those points are considered duplicated, and one will be removed.
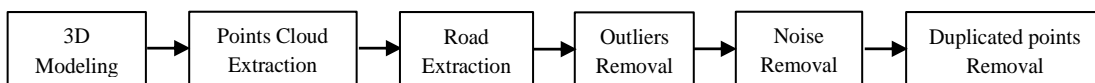
3D Modeling	→	Points Cloud Extraction	→	Road Extraction	→	Outliers Removal	→	Noise Removal	→	Duplicated points Removal

Figure 2. Data processing

3.4. Road segmentation

The objective is to segment the remaining 3D points from data processing into two groups: 3D points representing non-distressed areas and points representing distress. This step consists of three sub-steps, as illustrated in Figure 3: normal plane definition, 3D points to normal plane distances calculation, and 3D points segmentation. The normal plane simulates the road surface before the damage. In this case, as the area to be inspected is small, a single normal plane was considered for the entire pavement section. This plane is fitted from processed 3D points using the PCA technique. PCA tries to find the plane representing the minimal root mean square (RMS) distances to all points. Then, distances between the normal plane and 3D points are calculated by making the vertical projection of a point to this plane. Finally, 3D points segmentation consists of clustering points, based on distances to the normal plane, into non-distressed 3D points (with distances less than 0.1 cm) and distressed 3D points (with distances greater than 0.1 cm).
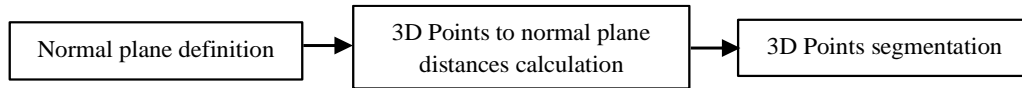
Normal plane definition	→	3D Points to normal plane distances calculation	→	3D Points segmentation

Figure 3. Road segmentation

4.   RESULTS AND DISCUSSION

This section summarizes and discusses the main findings of the work. The material used and the study area are described while mentioning the reason for those choices. The simulation results were obtained using the virtual environment Google Colab, which provides a memory RAM of up to 12 GB and a disk capacity of up to 120 GB.

4.1. Material
4.1.1. Unmanned aerial vehicle

An in-depth study evaluated all DJI family UAVs and determined the most suitable drone to provide high-quality images that meet 3D modeling requirements, as described in Table 2. This study evaluated various factors, such as image resolution, sensor size, maximum speed, and flight time. After a thorough analysis, it was concluded that the MAVIC AIR 2 is the most appropriate UAV prototype for this study. This UAV has a high-quality camera (48 MP and 1/2" sensor size) that can collect high-quality images with a good resolution, providing more accurate and reliable data for pavement 3D representation and segmentation. Other characteristics of this UAV, such as maximum speed (19 m/s) and maximum flight time (34 min), also make it a suitable option for this study.

4.1.2. Camera

The camera chosen for the study is the commercial EOS 450D manufactured by Canon. The advantages of this camera are its low cost, reliability, reasonable resolution of 12.2 MP, and the ability to provide images that meet pavement 3D modeling requirements. Table 3 summarizes the most important characteristics of this camera.

Table 2. DJI UAVs family characteristics

Series	Type	Weight (g)	Dimensions (L×W×H) (mm)³	Max Speed (m/s)	Max Flight Time (min)	Camera Sensor CMOS	Resolution (MP)
MAVIC	DJI AIR 2S	595	183×253×77	19	31	1"	20
	AIR 2	**570**	**183×253×77**	**19**	**34**	**1/2"**	**48**
	MINI	249	245×289×55	13	30	1/2.3"	12
	2 PRO	907	322×242×84	20	31	1"	20
	2 ZOOM	905	322×242×84	20	31	1/2.3"	12
	2 ENTERPRISE ADVANCED	1 100	322×242×84	20	31	1/2"	48
	2 ENTERPRISE SERIES	1 100	322×242×84	20	31	1 100	12
	AIR	430	168×184×64	19	21	1/2.3"	12
	Pro Platinum	743	83×83×198	18	30	1/2.3"	12.35
	Mavic Pro	743	83×83×198	18	27	1/2.3"	12.35
	DJI MINI 2	< 249	159×203×56	16	31	1/2.3"	12
	DJI MINI 2 (JP VERSION)	199	159×202×55	16	18	1/2.3"	12
SPARK	SPARK	300	143×143×55	14	16	1/2.3"	12
PHANTOM	4 PRO V2.0	1 388		20	30	1"	20
	4 PRO	1 388		20	30	1"	20
	4 ADVANCED	1 388		20	30	1"	20
	4 RTK	1 391		16	30	1"	20
	4	1 380		20	28	1/2.3"	12
	3 4K	1 280		16	25	1/2.3"	12.4
	3 SE	1 236		16	25	1/2.3"	12
	3 PROFESSIONAL	1 280		16	23	1/2.3"	12.4
	3 ADVANCED	1 280		16	23	1/2.3"	12.4
	3 STANDARD	1 216		16	25	1/2.3"	12
FPV	FPV	795	255×312×127	39	20	1/2.3"	12
MATRICE	300 RTK	9 000	810×670×430	23	45		
	200 V2	6 140	883×886×398	22.5	38		
	210 V2	6 140	883×886×398	22.5	34		
	210 RTK V2	6 140	883×886×427	22.5	33		
	200	6 140	716×220×236	23	27		

*Data in bold corresponds to the UAV chosen for the study.
*Missing data needs to be illustrated in the manufactured manuals.

Table 3. EOS 450D camera characteristics

Characteristic	Description
Type	Digital mono-objective AF/AE with a built-in flash.
Recording	Memory cards: SD and SDHC
Sensor size	22.2×14.8 mm
Sensor Type	CMOS
Resolution	12, 20 Mega Pixels
Recording format	File System 2.0
Image types	JPEG, RAW and simultaneous (JPEG + RAW)
Display	LCD with 3.0 po
Battery	LP-E5: 7.4 V and 1080 mAh
Number of pictures	400 – 600 photos
Dimensions (L×H×P)	128.8×97.5×61.9 mm
Weight	475 g
Temperature	0 °C - 40 °C
Humidity	< 85 %

4.2. Study area

The study area is located in the city of Kenitra, Morocco. Road conditions in this city are not excellent because of several parameters, predominantly temperature change, humidity, and heavy vehicles transporting products to the port of Kenitra. The humidity effect is due to the city's position near the Atlantic Ocean; the river of 'Sebou' flows through the city and the lake 'Sidi Boughaba.' Despite administration representatives' efforts to maintain the road condition in good shape, some sections still present critical situations and need to be maintained. The selected road was constructed based on the asphalt near Ibn Tofail University. A pavement segment from the east road connecting the university to the city's center is selected as a case study, as shown in Figure 4. This segment is 3m long and presents a complex distressed area that combines two potholes and one rut. This segment was selected because it exemplifies the broader road challenges faced by Kenitra City, thus making it an ideal candidate for an in-depth case study.
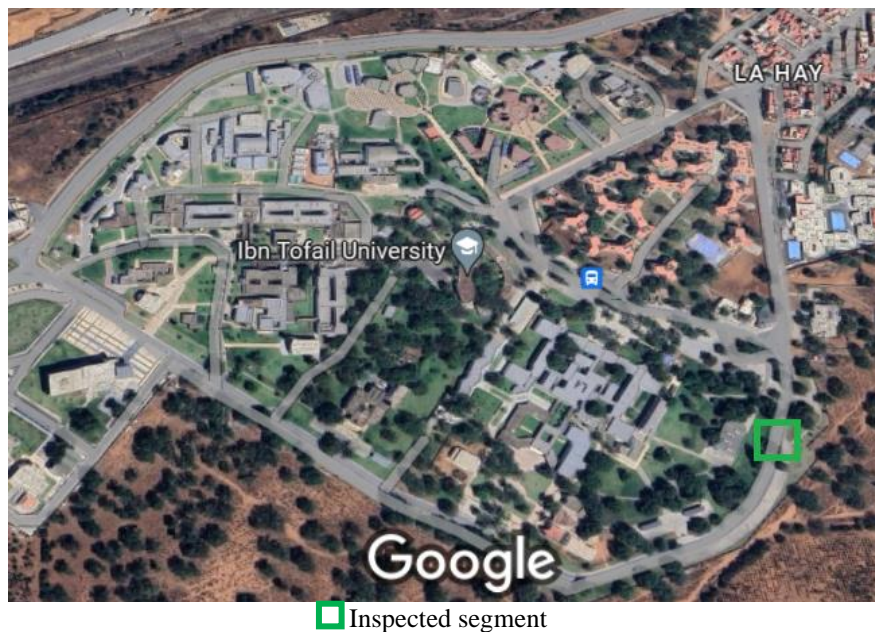

☐ Inspected segment

Figure 4. The location of the study area

4.3. Data acquisition

As a first step to validate the proposed method, the EOS 450D camera was used to take pictures of the selected section of the pavement. The survey was conducted on the 13th of August 2022 during daylight hours (between 11:00 am and 01:00 pm) to ensure clear and not blurred images. The environmental conditions at this time were as follows: temperature=27 °C, wind speed=14 Km/h north-west and humidity=70%. The camera

was set to automatic mode, allowing all parameters to be automatically adjusted. During the data acquisition, distances between the camera and the pavement surface were kept within the range of 1 to 2 meters to maintain a good resolution. Twenty-three (23) images were taken from different angles while covering all possible views, as shown in Figures 5 and 6. Images were saved in a JPG format with 4272×2848 pixels.
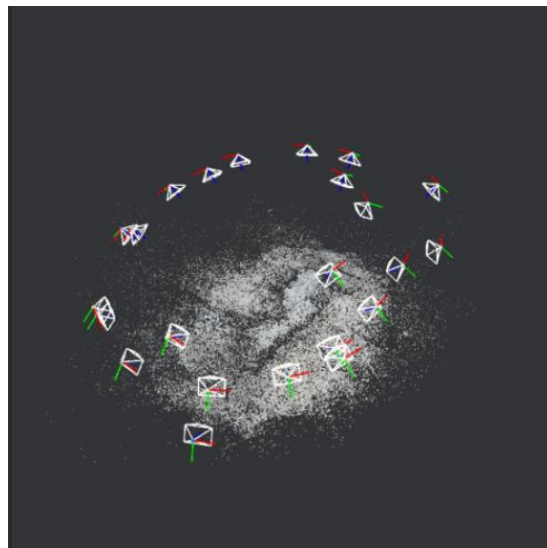

Figure 5. Images captured during the survey

Figure 6. Camera poses during data acquisition

4.4. Simulation

3D modeling of the selected road section was created by importing the 23 captured images to a personalized version of Meshroom that was adapted and run on a virtual machine via Google Colab to reduce simulation time and overcome computer limitations. The environment provided by Google Colab consists of a memory RAM of up to 12 GB and a disk capacity of up to 120 GB. Simulation time was 30 minutes to generate the 3D model in the OBJECT format (.OBJ) and textures in two images with the portable network graphics format (.PNG).

After that, the OBJ file was imported to CloudCompare for visualization and data processing. Figure 7 illustrates the 3D model shape variation during the data processing sub-steps. The 3D model was created in a mesh format containing 817,370 points and 1,633,819 meshes (triangles) as shown in Figure 7(a). By applying the points sampling method, 800,177 points were extracted from the 3D model as shown in Figure 7(b). Then, the SOR filter was applied to those points. In this case, the values of K and N were set to 6 and 1, respectively. As a result, 677,625 points were kept as shown in Figure 7(c). After that, a noise filter was applied by setting the sphere's radius to 0.9 cm and the maximum error to 1, which resulted in 395,517 remaining points as shown in Figure 7(d). Isolated points were removed during noise filtering by removing all points with less than three neighbors inside the defined sphere. Finally, 69 duplicated points were removed to leave 395,448 as shown in Figure 7(e).
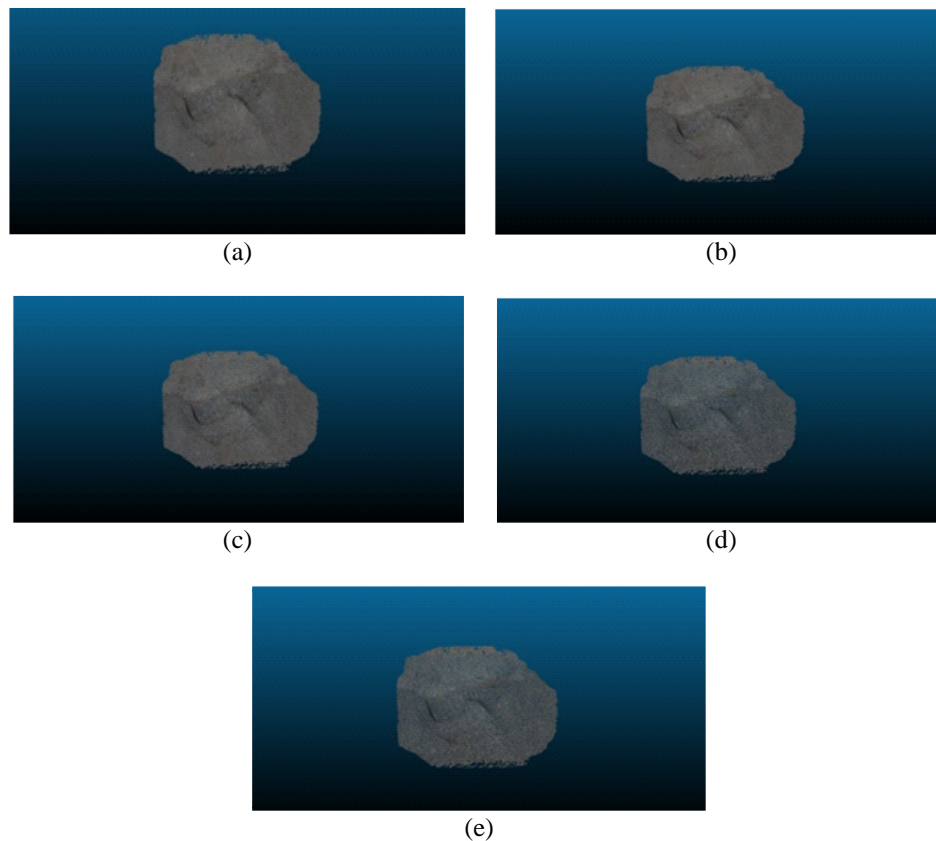

(a)

(b)

(c)

(d)

(e)

Figure 7. Variation of 3D model shape through data processing steps (a) initial 3D model with meshes, (b) point clouds sampling, (c) SOR filtering, (d) noise filtering, and (e) duplicated points removal

A plane was fitted to the remaining 395,448 points by using the PCA technique. This plane is considered the normal plane for the pavement. After that, distances between each point and the fitted plan are calculated. These distances ranged between -2.06 and 3.11 cm. Red and orange represent points with distances from the normal plane between 2 and 3.11 cm. The yellow color is considered for points with distances from the normal plane between 1 and 2 cm. The green color is considered for points with distances from the normal plane between -0.78 and 1 cm. The blue represents points with distances from the normal plane between -2.06 and -0.78 cm. Figure 8 illustrates the location of the distressed area, Figure 8(a) shows the normal plane position through 3D points representing the pavement segment of the study, and Figure 8(b) illustrates the variation of distances between the normal plane and those points.

After that, a filter was applied to segment the road into distressed and non-distressed areas as shown in Figure 9. This filter clusters 3D points into two groups based on their distances from the normal plane. Distressed areas, as illustrated in Figure 9(a), are represented by 3D points with distances to the normal plane more than 1 cm, and non-distressed areas as shown in Figure 9(b) are formed by 3D points with distances less than 1 cm to the normal plane.
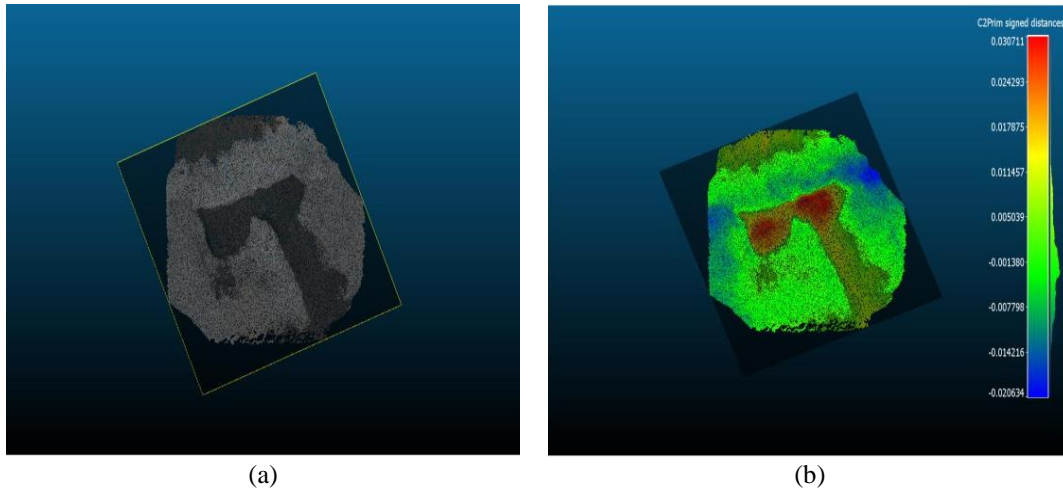
(a)   (b)

Figure 8. The location of the distressed area (a) normal plane estimation and (b) 3D points to normal plane distance variation

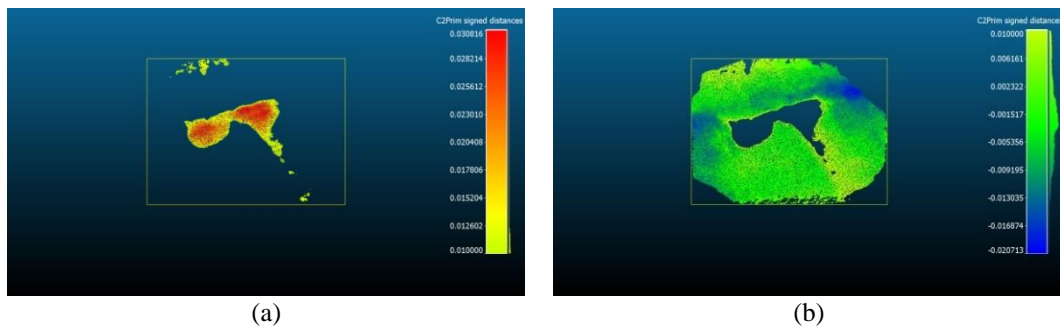(a)   (b)

Figure 9. Road segmentation (a) distressed areas and (b) non-distressed areas

4.5. Discussion

The proposed method was applied to a section of pavement for 3D representation and road segmentation to distressed and non-distressed areas. Twenty-three (23) images on a JPG format were taken by the commercial camera EOS 450D with a good resolution of 4272×2848 pixels. Those images were transferred to a 3D model containing 817,370 points and 1,633,819 meshes (triangles). After data processing, all meshes and 421,922 points (51.62% of the initial 3D model) were removed, as shown in Table 4. Then, a plane was fitted to the remaining 395,448 points. The root mean square of distances between each remaining points and the normal plane was RMS=0.85 cm. The most deviated points are represented by red, followed by yellow, and the green color represents minor deviations. However, the blue color characterizes points with an elevation higher than the normal plane. Figure 10 describes the histogram of colors representing distances between each remaining point and the normal plane. The proposed method successfully creates a 3D model and segments the road into non-distressed and distressed areas. The rate of similarity to the survey measurement passed 95%.

However, this method was applied to a minor road section containing two types of distress (pothole and rut). It should be enhanced to detect, with high accuracy, minor damages and other distress types such as cracks. The method should also be adapted to handle extended road networks by estimating the normal plane locally while considering the variation of the road curvature. The proposed approach makes semi-automatic distress detection; distressed areas are detected automatically. However, the type of distress is defined by a visual observation, which could be improved by developing an algorithm to automate the process.

The proposed approach presents a crucial milestone in the global study 'Automated pavement distress detection, classification, and measurement'. The results prove that the proposed solution is efficient and most advantageous regarding its low cost and the possibility of enhancing several steps. Future research will focus on enhancing the accuracy and automating distress detection, measurement, and classification. The method will also be adapted to handle an extensive network of roads while using UAVs for data acquisition.

Table 4. 3D Points numbers variation through the data processing sub-steps

Step	Number of points	Number of removed points
3D model with meshes	817 370	0
Points sampling	800 177	17 193
SOR filter application	677 625	122 552
Noise filter application and isolated points removal	395 517	282 108
Duplicated points removal	395 448	69
Total points removed		421 922
Percentage of total points removed		51.62 %
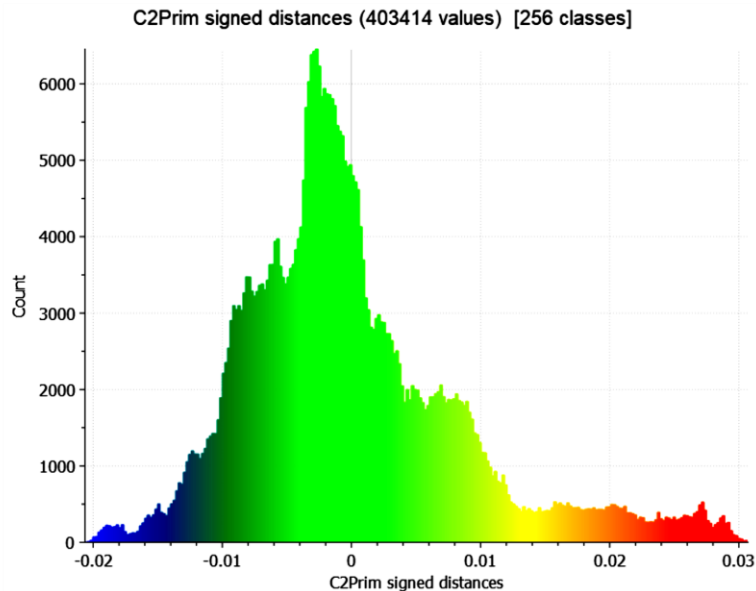
Figure 10. Histogram of remaining points to normal plane distances

5. CONCLUSION

This study presents a low-cost and quick solution based on an unmanned aerial vehicle, a commercial camera, and the Structure from Motion technique for the 3D representation and segmentation of road sections. The EOS 450D camera was used to capture images of the pavement from different angles with an overlap of 70 %. Those images were used to create a road 3D model using a personalized version of Meshroom based on SFM. Then, points sampled from the 3D model are processed by applying the Statistical Outlier Removal and noise filters to remove unnecessary data. After that, isolated and duplicated points were eliminated based on a minimal distance from neighbors. The normal plane, which represents the road surface before the damage, was fitted from the remaining points using the principal component analysis technique. Then, distances between each point and the normal plane were calculated and clustered to segment the road into distressed and non-distressed areas. In order to validate this approach, a case study has been conducted in a road section near Ibn Tofail University, Kenitra, Morocco. Based on a comparison between results obtained from simulation and survey measurements, it was observed that the proposed method is accurate in road 3D modeling and segmentation for complicated distress in the pavement, including depth information. The rate of similarity passed 95%. Future works will focus on improving the proposed approach by automating detection, measurement, and classification in an extensive network of roads.

REFERENCES

[1] R. Roberts, L. Inzerillo, and G. Di Mino, "Developing a framework for using structure-from-motion techniques for road distress applications," *European Transport - Trasporti Europei*, no. 77, pp. 1–11, 2020, doi: 10.48295/et.2020.77.5.

[2] B. Benmhahe and J. A. Chentoufi, "Automated pavement distress detection, classification and measurement: a review," *International Journal of Advanced Computer Science and Applications*, vol. 12, no. 8, pp. 708–718, 2021, doi: 10.14569/IJACSA.2021.0120882.

[3] N. Sholevar, A. Golroo, and S. R. Esfahani, "Machine learning techniques for pavement condition evaluation," *Automation in Construction*, vol. 136, 2022, doi: 10.1016/j.autcon.2022.104190.

[4] Z. Xiong, H. Sheng, W. G. Rong, and D. E. Cooper, "Intelligent transportation systems for smart cities: a progress review," *Science China Information Sciences*, vol. 55, no. 12, pp. 2908–2914, 2012, doi: 10.1007/s11432-012-4725-1.

[5]   T. B. J. Coenen and A. Golroo, "A review on automated pavement distress detection methods," *Cogent Engineering*, vol. 4, no. 1, Art. no. 1374822, 2017, doi: 10.1080/23311916.2017.1374822.

[6]   A. Ragnoli, M. R. De Blasiis, and A. Di Benedetto, "Pavement distress detection methods: a review," *Infrastructures*, vol. 3, no. 4, 2018, doi: 10.3390/infrastructures3040058.

[7]   Z. Tong, D. Yuan, J. Gao, and Z. Wang, "Pavement defect detection with fully convolutional network and an uncertainty framework," *Computer-Aided Civil and Infrastructure Engineering*, vol. 35, no. 8, pp. 832–849, 2020, doi: 10.1111/mice.12533.

[8]   W. Song, G. Jia, H. Zhu, D. Jia, and L. Gao, "Automated pavement crack damage detection using deep multiscale convolutional features," *Journal of Advanced Transportation*, vol. 2020, pp. 1–11, 2020, doi: 10.1155/2020/6412562.

[9]   Q. Mei and M. Gül, "Multi-level feature fusion in densely connected deep-learning architecture and depth-first search for crack segmentation on images collected with smartphones," *Structural Health Monitoring*, vol. 19, no. 6, pp. 1726–1744, 2020, doi: 10.1177/1475921719896813.

[10] Q. Mei and M. Gül, "A cost effective solution for pavement crack inspection using cameras and deep neural networks," *Construction and Building Materials*, vol. 256, 2020, doi: 10.1016/j.conbuildmat.2020.119397.

[11] Z. Fan *et al.*, "Ensemble of deep convolutional neural networks for automatic pavement crack detection and measurement," *Coatings*, vol. 10, no. 2, p. 152, 2020, doi: 10.3390/coatings10020152.

[12] J. Lekshmipathy, N. M. Samuel, and S. Velayudhan, "Vibration vs. vision: best approach for automated pavement distress detection," *International Journal of Pavement Research and Technology*, vol. 13, no. 4, pp. 402–410, 2020, doi: 10.1007/s42947-020-0302-y.

[13] H. Bello-Salau, A. J. Onumanyi, B. O. Sadiq, H. Ohize, A. T. Salawudeen, and A. M. Aibinu, "An Adaptive wavelet transformation filtering algorithm for improving road anomaly detection and characterization in vehicular technology," *International Journal of Electrical and Computer Engineering (IJECE)*, vol. 9, no. 5, pp. 3664–3670, 2019, doi: 10.11591/ijece.v9i5.pp3664-3670.

[14] V. M. A. Souza, "Asphalt pavement classification using smartphone accelerometer and complexity invariant distance," *Engineering Applications of Artificial Intelligence*, vol. 74, pp. 198–211, 2018, doi: 10.1016/j.engappai.2018.06.003.

[15] D. A. Casas-Avellaned and J. F. López-Parra, "Detection and localization of road imperfections using smartphones (in Spain)," *DYNA (Colombia)*, vol. 83, no. 195, pp. 156–162, 2016, doi: 10.15446/dyna.v83n195.44919.

[16] L. Forslöf and H. Jones, "Roadroid: continuous road condition monitoring with smart phones," *Journal of Civil Engineering and Architecture*, vol. 9, no. 4, 2015, doi: 10.17265/1934-7359/2015.04.012.

[17] Y. Du, N. Pan, Z. Xu, F. Deng, Y. Shen, and H. Kang, "Pavement distress detection and classification based on YOLO network," *International Journal of Pavement Engineering*, vol. 22, no. 13, pp. 1659–1672, 2021, doi: 10.1080/10298436.2020.1714047.

[18] Y. Wang, K. Song, J. Liu, H. Dong, Y. Yan, and P. Jiang, "RENet: rectangular convolution pyramid and edge enhancement network for salient object detection of pavement cracks," *Measurement: Journal of the International Measurement Confederation*, vol. 170, 2021, doi: 10.1016/j.measurement.2020.108698.

[19] P. K. Saha, D. Arya, A. Kumar, H. Maeda, and Y. Sekimoto, "Road rutting detection using deep learning on images," in *Proceedings - 2022 IEEE International Conference on Big Data, Big Data 2022*, 2022, pp. 1362–1368, doi: 10.1109/BigData55660.2022.10020458.

[20] R. Nyirandayisabye, H. Li, Q. Dong, T. Hakuzweyezu, and F. Nkinahamira, "Automatic pavement damage predictions using various machine learning algorithms: evaluation and comparison," *Results in Engineering*, vol. 16, 2022, doi: 10.1016/j.rineng.2022.100657.

[21] A. H. El Hakea and M. W. Fakhr, "Recent computer vision applications for pavement distress and condition assessment," *Automation in Construction*, vol. 146, 2023, doi: 10.1016/j.autcon.2022.104664.

[22] J. Liu *et al.*, "Automated pavement crack detection and segmentation based on two-step convolutional neural network," *Computer-Aided Civil and Infrastructure Engineering*, vol. 35, no. 11, pp. 1291–1305, 2020, doi: 10.1111/mice.12622.

[23] Y. Hou *et al.*, "The state-of-the-art review on applications of intrusive sensing, image processing techniques, and machine learning methods in pavement monitoring and analysis," *Engineering*, vol. 7, no. 6, pp. 845–856, 2021, doi: 10.1016/j.eng.2020.07.030.

[24] A. Dipankar and S. K. Suman, "Pavement crack detection based on a deep learning approach and visualisation by using GIS," *International Journal of Pavement Engineering*, vol. 24, no. 1, 2023, doi: 10.1080/10298436.2023.2173754.

[25] M. Zhong, L. Sui, Z. Wang, and D. Hu, "Pavement crack detection from mobile laser scanning point clouds using a time grid," *Sensors*, vol. 20, no. 15, pp. 1–20, 2020, doi: 10.3390/s20154198.

[26] S. Mathavan, K. Kamal, and M. Rahman, "A review of three-dimensional imaging technologies for pavement distress detection and measurements," *IEEE Transactions on Intelligent Transportation Systems*, vol. 16, no. 5, pp. 2353–2362, 2015, doi: 10.1109/TITS.2015.2428655.

[27] Y. C. J. Tsai and F. Li, "Critical assessment of detecting asphalt pavement cracks under different lighting and low intensity contrast conditions using emerging 3D laser technology," *Journal of Transportation Engineering*, vol. 138, no. 5, pp. 649–656, 2012, doi: 10.1061/(ASCE)TE.1943-5436.0000353.

[28] S. Bruno *et al.*, "A robotized Raspberry-based system for pothole 3D reconstruction and mapping," *Sensors*, vol. 23, no. 13, Art. no. 5860, 2023, doi: 10.3390/s23135860.

[29] S. Biçici and M. Zeybek, "An approach for the automated extraction of road surface distress from a UAV-derived point cloud," *Automation in Construction*, vol. 122, 2021, doi: 10.1016/j.autcon.2020.103475.

[30] C. Zhang and A. Elaksher, "3D reconstruction from UAV-acquired imagery for road surface distress assessment," in *31st Asian Conference on Remote Sensing 2010*, 2010, vol. 1, pp. 386–391.

[31] R. J. Dobson, C. Brooks, C. Roussi, and T. Colling, "Developing an unpaved road assessment system for practical deployment with high-resolution optical data collection using a helicopter UAV," in *2013 International Conference on Unmanned Aircraft Systems, ICUAS 2013 - Conference Proceedings*, 2013, pp. 235–243, doi: 10.1109/ICUAS.2013.6564695.

[32] R. Roberts, L. Inzerillo, and G. Di Mino, "Using UAV Based 3D Modelling to Provide Smart Monitoring of Road Pavement Conditions," *Information 2020, Vol. 11, Page 568*, vol. 11, no. 12, p. 568, 2020, doi: 10.3390/INFO11120568.

[33] M. Zeybek and S. Biçici, "Road distress measurements using UAV," *Turkish Journal of Remote Sensing and GIS*, vol. 1, no. 1, pp. 13–23, 2020.

[34] Y. Tan and Y. Li, "UAV photogrammetry-based 3D road distress detection," *ISPRS International Journal of Geo-Information*, vol. 8, no. 9, 2019, doi: 10.3390/ijgi8090409.

[35] G. Leonardi, V. Barrile, R. Palamara, F. Suraci, and G. Candela, "3D mapping of pavement distresses using an unmanned aerial vehicle (UAV) system," in *Smart Innovation, Systems and Technologies*, vol. 101, Springer International Publishing, 2019, pp. 164–171.

[36] A. M. Saad and K. N. Tahar, "Identification of rut and pothole by using multirotor unmanned aerial vehicle (UAV)," *Measurement: Journal of the International Measurement Confederation*, vol. 137, pp. 647–654, 2019, doi: 10.1016/j.measurement.2019.01.093.

[37] L. Inzerillo, G. Di Mino, and R. Roberts, "Image-based 3D reconstruction using traditional and UAV datasets for analysis of road pavement distress," *Automation in Construction*, vol. 96, pp. 457–469, 2018, doi: 10.1016/j.autcon.2018.10.010.

[38] R. Roberts, L. Inzerillo, and G. Di Mino, "Exploiting Low-Cost 3D Imagery for the Purposes of Detecting and Analyzing Pavement Distresses," *Infrastructures 2020, Vol. 5, Page 6*, vol. 5, no. 1, 2020, doi: 10.3390/INFRASTRUCTURES5010006.

[39] A. Schmidt and D. Aufderheide, "Application of inventive design methodology for a sensor fusion approach in structure-from-motion (SfM) applications," in *2022 1st International Conference on Information System and Information Technology*, 2022, pp. 431–436, doi: 10.1109/ICISIT54091.2022.9872690.

[40] P. An, K. Fang, Q. Jiang, H. Zhang, and Y. Zhang, "Measurement of rock joint surfaces by using smartphone structure from motion (SfM) photogrammetry," *Sensors*, vol. 21, no. 3, pp. 1–22, 2021, doi: 10.3390/s21030922.

[41] J. L. Schonberger and J.-M. Frahm, "Structure-from-motion revisited," in *2016 IEEE Conference on Computer Vision and Pattern Recognition (CVPR)*, 2016, pp. 4104–4113, doi: 10.1109/CVPR.2016.445.

[42] C. Wu, "VisualSFM: a visual structure from motion system." http://ccwu.me/vsfm/index.html (accessed Sep. 11, 2023).

[43] N. Snavely, "Bundler: structure from motion (SfM) for unordered image collections," Computer Science at Cornell University, https://www.cs.cornell.edu/~snavely/bundler/#S3 (accessed Sep. 11, 2023).

[44] PIX4D, "PIX4Dmapper-Support," PIX4D https://support.pix4d.com/hc/en-us/categories/360001503192 (accessed Dec. 18, 2023).

[45] Epic Developer Community "Capturing Reality," Epic Games, https://dev.epicgames.com/community/capturing-reality/getting-started/reality-capture (accessed Dec. 18, 2023).

[46] Agisoft, "Agisoft Metashape: User Manuals." Agisoft, Accessed Sep. 11, 2023. [Online]. Available: https://www.agisoft.com/downloads/user-manuals/.

[47] "Meshroom - 3D reconstruction software," *AliceVision*. https://alicevision.org/#meshroom (accessed Sep. 11, 2023).

[48] "Google colaboratory," *Google Colab*. https://colab.research.google.com/notebooks/basic_features_overview.ipynb (accessed Dec. 18, 2023).

[49] "CloudCompare Wiki." CloudCompare, https://www.cloudcompare.org/doc/wiki/index.php/Main_Page (accessed Dec. 18, 2023).

BIOGRAPHIES OF AUTHORS

Brahim Benmhahe telecommunication engineer since 2010. He is also a Ph.D. student at Ibn Tofail University, Kenitra, Morocco, since 2021. His research interests include pavement health monitoring, machine learning, points cloud manipulation, and 3D modeling. He can be contacted at email: Brahim.benmhahe@uit.ac.ma.

Jihane Alami Chentoufi professor and Ph.D. supervisor in the Research on Computer Science Laboratory at Ibn Tofail University, Faculty of Sciences-Kenitra. She received her M.S. and Ph.D. in computer sciences from Mohammed V University, Faculty of Sciences-Rabat, Morocco, in 2003 and 2007, respectively. Her main research interests include metaheuristics, combinatorial optimization, and decision-making problems. She can be contacted at email: J.alami@uit.ac.ma.

Mohamed Amine Basmassi Ph.D. in 2023, research assistance at Ibn Tofail University, Kenitra, Morocco. In 2015, he received the M.S. in computer engineering from Abdelmalek Essaadi University, Tetouan, Morocco. In 2012, he had a B.S. degree in fundamental mathematics and computer science from Cadi Ayyad University, Marrakech-Safi, Morocco. His research interests fall in machine learning, heuristic techniques, computational intelligence, and multi-agent systems to solve problems related to transport and traffic management, combinatorial optimization, and decision-making problems. He can be contacted at email: Basmassi.med.amine@gmail.com.